

# CFD Simulation of Fruit Fly Wing Beat Motion

An investigation of unsteady aerodynamics of fruit-fly wing motion to determine passiveness of different degrees of freedom

A Chalmers University of Technology Report for TRA270 Track Course - Fluid Structure Interactions, Study Period 2

BALA KUMARESH THILEEP KUMAR  
CHAITHANYA KARRA  
JOHN PAUL PERUMADAN MANNUMMAL  
RAJ GOPALA KRISHNA SUBRAMANI VENKATACHALAM  
SHREEYESH SREENIVASAN



# PROJECT REPORT 2025

## CFD Simulation of Fruit Fly Wing Beat Motion

An investigation of unsteady aerodynamics of fruit-fly wing motion  
to determine passiveness of different degrees of freedom

BALA KUMARESH THILEEP KUMAR

CHAITHANYA KARRA

JOHN PAUL PERUMADAN MANNUMMAL

RAJ GOPALA KRISHNA SUBRAMANI VENKATACHALAM

SHREEYESH SREENIVASAN



UNIVERSITY OF  
GOTHENBURG



**CHALMERS**  
UNIVERSITY OF TECHNOLOGY

Department of Mechanics and Maritime Sciences  
CHALMERS UNIVERSITY OF TECHNOLOGY  
UNIVERSITY OF GOTHENBURG  
Gothenburg, Sweden 2025

CFD Simulation of Fruit Fly Wing Beat Motion

An investigation of unsteady aerodynamics of fruit-fly wing motion to determine passiveness of different degrees of freedom

BALA KUMARESH THILEEP KUMAR

CHAITHANYA KARRA

JOHN PAUL PERUMADAN MANNUMMAL

RAJ GOPALA KRISHNA SUBRAMANI VENKATACHALAM

SHREEYESH SREENIVASAN

© BALA KUMARESH THILEEP KUMAR

CHAITHANYA KARRA

JOHN PAUL PERUMADAN MANNUMMAL

RAJ GOPALA KRISHNA SUBRAMANI VENKATACHALAM

SHREEYESH SREENIVASAN, 2025.

Supervisor: Arion Pons, Division of Fluid Dynamics, Department of Mechanics and Maritime Sciences

Examiner: Hua-Dong Yao, Department of Mechanics and Maritime Sciences

Project Report 2025

Department of Mechanics and Maritime Sciences

Chalmers University of Technology and University of Gothenburg

SE-412 96 Gothenburg

Telephone +46 31 772 1000

Cover: Velocity contour plots of an instance from CFD simulation

Typeset in L<sup>A</sup>T<sub>E</sub>X

Gothenburg, Sweden 2025

# CFD Simulation of Fruit Fly Wing Beat Motion

An investigation of unsteady aerodynamics of fruit-fly wing motion to determine passiveness of different degrees of freedom

BALA KUMARESH THILEEP KUMAR

CHAITHANYA KARRA

JOHN PAUL PERUMADAN MANNUMMAL

RAJ GOPALA KRISHNA SUBRAMANI VENKATACHALAM

SHREEYESH SREENIVASAN

Department of Mechanics and Maritime Sciences

Chalmers University of Technology and University of Gothenburg

## Abstract

In this report, results from an investigation carried out using CFD on the unsteady aerodynamics of rigid fruit fly wing executing hovering motion is presented. The work was primarily aimed at determining the degree of passiveness of different degrees of freedom involved in the fruit fly wing beat cycle. Adhering to the kinematics obtained from literature, the wing beat cycle was simulated and studied using CFD software. The aerodynamic characteristics calculated from CFD is discussed. The results indicates the active nature of stroke and pitch motions involved in the wing beat motion. The findings from the study also suggests the presence of a partially active elevation motion at the extremes of strokes and this has to be further investigated. A fully coupled CFD simulation can be used to validate findings from this report.

Keywords: Fruit fly, Flapping wing, CFD, Unsteady aerodynamics, Overset mesh, Active and passive motion.



## **Acknowledgements**

We thank our supervisors, for guiding and supporting us through the project.

BALA KUMARESH THILEEP KUMAR  
CHAITHANYA KARRA  
JOHN PAUL PERUMADAN MANNUMMAL  
RAJ GOPALA KRISHNA SUBRAMANI VENKATACHALAM  
SHREEYESH SREENIVASAN

Gothenburg, July 2025



# Contents

<b>List of Figures</b>	<b>xi</b>
<b>1 Introduction</b>	<b>1</b>
1.1 General Scope . . . . .	1
1.2 Methodology . . . . .	2
1.3 Expected Outcomes . . . . .	2
<b>2 Theory</b>	<b>3</b>
2.1 Overview of CFD . . . . .	3
2.2 Overview of FSI . . . . .	4
2.3 Degree of Freedom . . . . .	4
2.3.1 Euler Angles . . . . .	4
2.4 Aerodynamic Forces and Moments . . . . .	5
2.4.1 Lift . . . . .	5
2.4.2 Drag . . . . .	5
2.4.3 Pitching Moment . . . . .	5
2.4.4 Stroke Moment . . . . .	6
2.4.5 Aerodynamic Work Loop . . . . .	6
2.5 Dynamic Stall & Vortex Shedding . . . . .	7
2.5.1 Dynamic Stall . . . . .	7
2.5.2 Vortex Shedding . . . . .	8
2.6 Overset Mesh . . . . .	8
2.7 Boundary Conditions Used in Simulation . . . . .	9
2.7.1 Stagnation Inlet . . . . .	9
2.7.2 Pressure Outlet . . . . .	9
2.8 $k - \omega$ Turbulence Model . . . . .	9
2.9 Drosophila Melanogaster (Fruit Fly) . . . . .	10
2.9.1 Fruit Fly Wing Kinematics . . . . .	10
<b>3 Methodology</b>	<b>13</b>
3.1 Pre-Processing . . . . .	13
3.1.1 Geometry Preparation . . . . .	13
3.1.2 Wing Kinematics Dataset for Simulation . . . . .	14
3.1.3 Computational Domain and Grid Generation . . . . .	14
3.1.4 Setting Up Wing Beat Motion in STAR-CCM+ . . . . .	18
3.2 Physics and Solver Setup . . . . .	21

3.3 Post-Processing . . . . .	22
<b>4 Results &amp; Summary</b>	<b>25</b>
4.1 Wing Beat Cycle Motion Analysis . . . . .	25
4.2 Aerodynamic Characteristics of Fruit Fly Wing Beat Motion . . . . .	26
4.2.1 Lift & Drag Characteristics . . . . .	27
4.2.2 Pitching Moment & Stroke Moment Characteristics . . . . .	28
4.3 Summary . . . . .	30

# List of Figures

2.1	Non-dimensionalized governing equations for incompressible flow . . . . .	3
2.2	Degrees of freedom in rotation . . . . .	4
2.3	Aerodynamic forces and pitching moment (negative) in airfoil . . . . .	6
2.4	Work loops: (A) positive work, (B) Near zero work, (c) Negative work	7
2.5	Dynamic stall stages taken from literature . . . . .	8
2.6	Overset mesh example from literature: Overset mesh setup for football moving in air . . . . .	9
2.7	Drosophila Melanogaster (Fruit Fly) . . . . .	10
2.8	Drosophila Melanogaster Wing Trajectory (top view) . . . . .	11
2.9	Drosophila Melanogaster Wing Trajectory (Wing tip view) . . . . .	11
3.1	Fruit fly wing geometry . . . . .	13
3.2	Computational domain used in simulation . . . . .	14
3.3	Steps to create computational domain . . . . .	15
3.4	Boundary conditions used at various region boundaries . . . . .	15
3.5	Steps to setting up boundary conditions . . . . .	16
3.6	Mesh control for overset mesh . . . . .	17
3.7	Computational grid . . . . .	17
3.8	Computational grid section view . . . . .	18
3.9	Laboratory and translating root-based Trajectory coordinate systems	18
3.10	Coordinate systems used to define motion . . . . .	19
3.11	Superimposed coordinate systems used to rotational motions . . . . .	19
3.12	Define translation and superimposing rotations . . . . .	19
3.14	Superimposed motion parameters . . . . .	20
3.13	Root translation parameters . . . . .	20
3.15	Rotation angle scalar function . . . . .	21
3.16	Motion specification to overset region . . . . .	21
3.17	Physics setup . . . . .	22
4.1	Variation of fruit fly wing Euler angles across wing beat cycle . . . . .	25
4.2	(a) Extremum of backward stroke (b) Intermediate position of forward stroke (c) Extremum of forward stroke (d) Intermediate position of backward stroke . . . . .	26
4.3	Lift profile over wing beat cycle . . . . .	27
4.4	Drag profile over wing beat cycle . . . . .	28
4.5	Pitching moment with respect to pitch angle variation over cycle . . . . .	28
4.6	Pitching moment hysteresis over a cycle . . . . .	29

## List of Figures

---

4.7	Stroke moment with respect to stroke angle variation over cycle . . . . .	30
4.8	Stroke moment hysteresis over a cycle .	30

# 1

## Introduction

In the vastness of entomology, the study of insect flight mechanics involving a beautifully orchestrated dance between muscles, exoskeleton and flexible wings has been a topic of interest in bio-mechanics research. Over the years, several research works have been trying to understand and learn from seemingly complex manoeuvres that defy the conventional notions of efficiency and performance carried out by insects[6, 9]. A set of muscles, exoskeletal structures, and wings known as the flight motor[19] play vital role in achieving this performance. Using different mechanisms across different species [20], the flight motor generates complex flapping wing beat kinematics [18, 14] which generate lift. The details of these kinematics are not fully understood[19]. Such interplay of active (due to muscle action) and passive elements (due to fluid-structure interaction) of the insect flight mechanics is particularly captivating of the seemingly common *Drosophila melanogaster* (*Fruit Fly*)[19]. Insects have a set of flight steering muscles to control their wing beat kinematics[1], but they also probably rely on passive fluid-structure interaction to generate certain kinematic features [2]. In particular, the wing pitch (or, incidence) degree of freedom (DOF) is thought to be passive in fruit flies [2] – but only on the basis of aerodynamic evidence from quasi-steady aerodynamic models. To confirm whether the pitch DOF is passive, we need higher-fidelity aerodynamic data, e.g. from CFD. In this report, an investigation carried out using CFD on the unsteady aerodynamics of a rigid fruit fly wing executing hovering motion is presented. The work was primarily aimed at determining the degree of passiveness of different degrees of freedom involved in the fruit fly wing beat cycle.

### 1.1 General Scope

Among different domains of applications, optimal control systems help achieve efficiency and performance in operation. Minimizing the number of active controls may reduce the chances of error and inefficiency in such systems. With this background, we have been looking into nature and studying different passive motions in it. In the present work, we focus on studying the complex wing beat motion of a fruit fly. The fruit fly wing beat is characterized to have three degrees of freedom namely pitch, stroke, and elevation [18]. The general scope of this study is to understand the complex wing beat motion and analyze the passiveness of different degrees of freedom.

We can approach the study in two ways. By an inverse approach where we it-

erate on stiffness damping properties of the fruit fly wing model until we achieve convergence with the observed kinematics. The second approach is where we use CFD to simulate the wing kinematics and find the stiffness and damping properties in different degrees of motion. In this work, we discuss and build on the CFD approach. The CFD approach is carried out using two types of simulations. First, the approach which is discussed in detail in this report is by considering a rigid fruit fly wing that follows the kinematics. The second approach where we do a fully coupled CFD simulation with flexible wings is considered as a future work. By simulating the aerodynamics of rigid fruit fly wings, we aim to identify the passiveness of pitch motion in particular.

## 1.2 Methodology

The kinematics of the fruit-fly wing motion is taken from literature [18, 14]. Fruit fly wing geometry is taken from literature[18]. The motion kinematics were defined using Fourier series approximations. The entire wing beat cycle was discretized and Euler angles for the wing for different instances along the discretized wing beat cycle are calculated from the Fourier approximations. This data is used to simulate and analyze the wing beat motion in CFD software. STAR-CCM+ software and cluster computing platforms were used for the simulations.

## 1.3 Expected Outcomes

Insights on different patterns of motions involved as well as concluding on the degree of passiveness of different degrees of freedom are the primary expected outcomes of this project. Also, We expect the simulations to aid in setting up a fully coupled simulation of the fruit fly wing and also to develop an accurate model of the complex fruit fly wing motion. The method used in this approach can be utilized to simulate and study similar unsteady flapping motions.

# 2

## Theory

In this chapter, a brief introduction to different concepts used to formulate the methodology and to analyze results are discussed. An overview of Computational Fluid Dynamics (CFD), Fluid Structure Interaction (FSI), Euler angles, active & passive motions, basic aerodynamic forces and moments, some basic understanding of unsteady aerodynamic phenomenon observed in results, regarding overset meshing, and finally some peculiarities of fruit fly wing kinematics are provided.

### 2.1 Overview of CFD

Computational fluid dynamics (CFD) is a branch of fluid mechanics that uses computer-based numerical analysis and algorithms to simulate, analyze, and solve problems in fluid flow. The discretized governing equations defining balance mass, momentum, and energy are solved to identify the physical state of flow in a computational domain. In the specific study, incompressible flow conditions are used since flow is characterized by low Reynolds number and negligible thermal effects. The non-dimensionalized continuity and Navier Stokes equations are shown in Fig.2.1.

$$\frac{\partial u}{\partial X} + \frac{\partial v}{\partial Y} + \frac{\partial w}{\partial Z} = 0,$$

$$\frac{\partial u}{\partial \tau} + u \frac{\partial u}{\partial X} + v \frac{\partial u}{\partial Y} + w \frac{\partial u}{\partial Z} = - \frac{\partial p}{\partial X} + \frac{1}{Re} \left( \frac{\partial^2 u}{\partial X^2} + \frac{\partial^2 u}{\partial Y^2} + \frac{\partial^2 u}{\partial Z^2} \right)$$

$$\frac{\partial v}{\partial \tau} + u \frac{\partial v}{\partial X} + v \frac{\partial v}{\partial Y} + w \frac{\partial v}{\partial Z} = - \frac{\partial p}{\partial Y} + \frac{1}{Re} \left( \frac{\partial^2 v}{\partial X^2} + \frac{\partial^2 v}{\partial Y^2} + \frac{\partial^2 v}{\partial Z^2} \right)$$

$$\frac{\partial w}{\partial \tau} + u \frac{\partial w}{\partial X} + v \frac{\partial w}{\partial Y} + w \frac{\partial w}{\partial Z} = - \frac{\partial p}{\partial Z} + \frac{1}{Re} \left( \frac{\partial^2 w}{\partial X^2} + \frac{\partial^2 w}{\partial Y^2} + \frac{\partial^2 w}{\partial Z^2} \right)$$

**Figure 2.1:** Non-dimensionalized governing equations for incompressible flow

## 2.2 Overview of FSI

Fluid Structural Interaction (FSI) is a set of problems within multiphysics modeling where coupling between fluid dynamics and structural mechanics are involved [17]. A quantitative understanding of biomechanics present in insects and birds in flight has been a major domain of FSI problems. Such problems are characterized by the action of hydrodynamic forces generated by the fluid over the wing deforming it and the deformed wing in turn affecting the flow. FSI problems are solved using coupled CFD solvers. Similar applications where FSI plays an important role in design considerations include systems like aircraft wings, wind turbine blades, blood flow in the human body, bridges, marine structures, and more.

## 2.3 Degree of Freedom

Degree of freedom refers to the number of possible ways a rigid object can move through space. A body in space has 6 degrees of freedom which corresponds to translation along the x,y, and z axis and rotations around the x,y, and z axis. In aerodynamics, the rotation around the x,y, and z axis are called roll, pitch, and yaw motions respectively as shown in Fig.2.2[22].

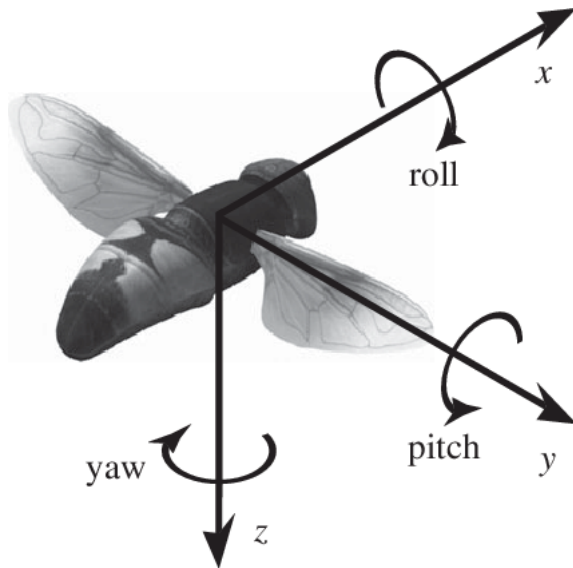


**Figure 2.2:** Degrees of freedom in rotation

### 2.3.1 Euler Angles

Euler angles include stroke angle ( $\psi$ ), pitch angle ( $\theta$ ) and elevation angle ( $\phi$ ). They are used in flapping kinematics to define the spatial orientation of the wing. Stroke angle also called sweeping angle is defined with respect to the z-axis. The pitch angle is defined with respect to the y-axis. Elevation angle is measured with respect to the x-axis.

## 2.4 Aerodynamic Forces and Moments

### 2.4.1 Lift

Lift is an aerodynamic force produced by the motion of a fluid past an object. Lift acts through the center of pressure of the object and is defined to be perpendicular to the flow direction.

The lift force is defined as:

$$F_L = 0.5 * \rho * A * C_L * V^2 \quad (2.1)$$

where,

( $\rho$ )-Density of fluid

( $A$ )-Cross sectional area

( $V$ )-Velocity of the object

( $C_L$ )-Coefficient of lift

### 2.4.2 Drag

Drag is an aerodynamic force produced by the relative motion of an object in a fluid. Drag acts parallel to the flow direction.

The Drag force is defined as:

$$F_D = 0.5 * \rho * A * C_D * V^2 \quad (2.2)$$

where,

$\rho$ -Density of fluid

$A$ -Cross sectional area

$V$ -Velocity of the object

$C_D$ -Coefficient of drag

### 2.4.3 Pitching Moment

The moment (or torque) produced by the lift force on an airfoil if that lift is considered to be applied, not at the center of pressure. The pitching moment is, by convention, considered to be positive when it acts to pitch the airfoil in the nose-up direction. This happens when the center of pressure is ahead of the center of gravity position along the chord line. Aerodynamic forces and pitching moment (negative) in airfoil is shown in Fig.2.3.[13]

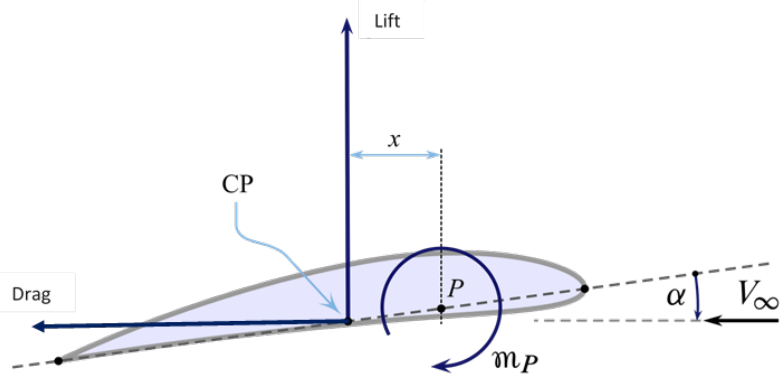


**Figure 2.3:** Aerodynamic forces and pitching moment (negative) in airfoil

#### 2.4.4 Stroke Moment

The moment (or torque) produced by the aerodynamic forces on a wing is measured with respect to the z-axis. The pitching moment is, by convention, considered to be positive when it acts counterclockwise.

#### 2.4.5 Aerodynamic Work Loop

The aerodynamic work loop in insect wings describes the energy transfer during flapping flight. As an insect wing oscillates, it undergoes positive and negative work phases, influencing lift and thrust generation. This cyclic process, depicted as a loop, captures the energy expenditure and transfer associated with wing motion. The concept aids in understanding the intricate aerodynamics and power requirements of insect flight, providing insights into the efficiency of their wing movements[5, 12]. Fig.2.4 shows work-loops observed in an insect muscle [7]

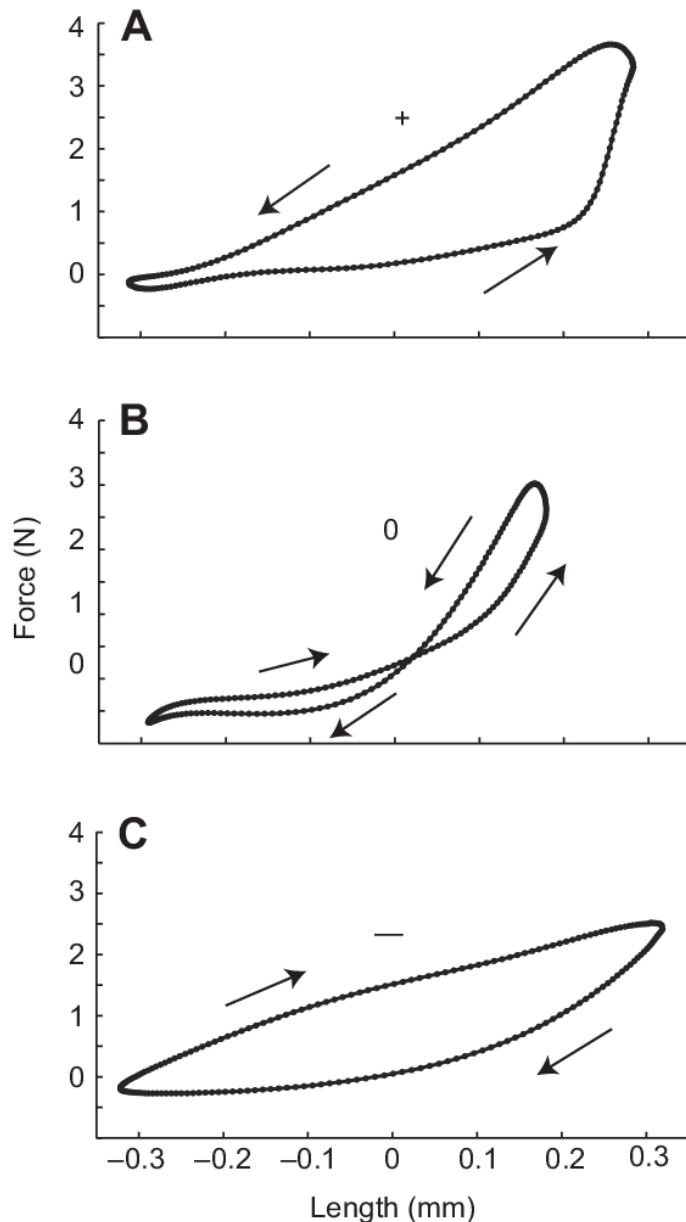


**Figure 2.4:** Work loops: (A) positive work, (B) Near zero work, (c) Negative work

## 2.5 Dynamic Stall & Vortex Shedding

### 2.5.1 Dynamic Stall

Dynamic stall is a complex fluid dynamics problem that occurs on an airfoil during rapid, transient motion in which the angle of attack goes beyond the static stall angle. The different stages of stall with variation of angle of attack in an airfoil is shown in Fig.2.5. [21].

### 2.5.2 Vortex Sheding

Vortex shedding is the periodic shedding of vortices behind an object in a fluid flow, typically occurring when an object obstructs the flow [10].

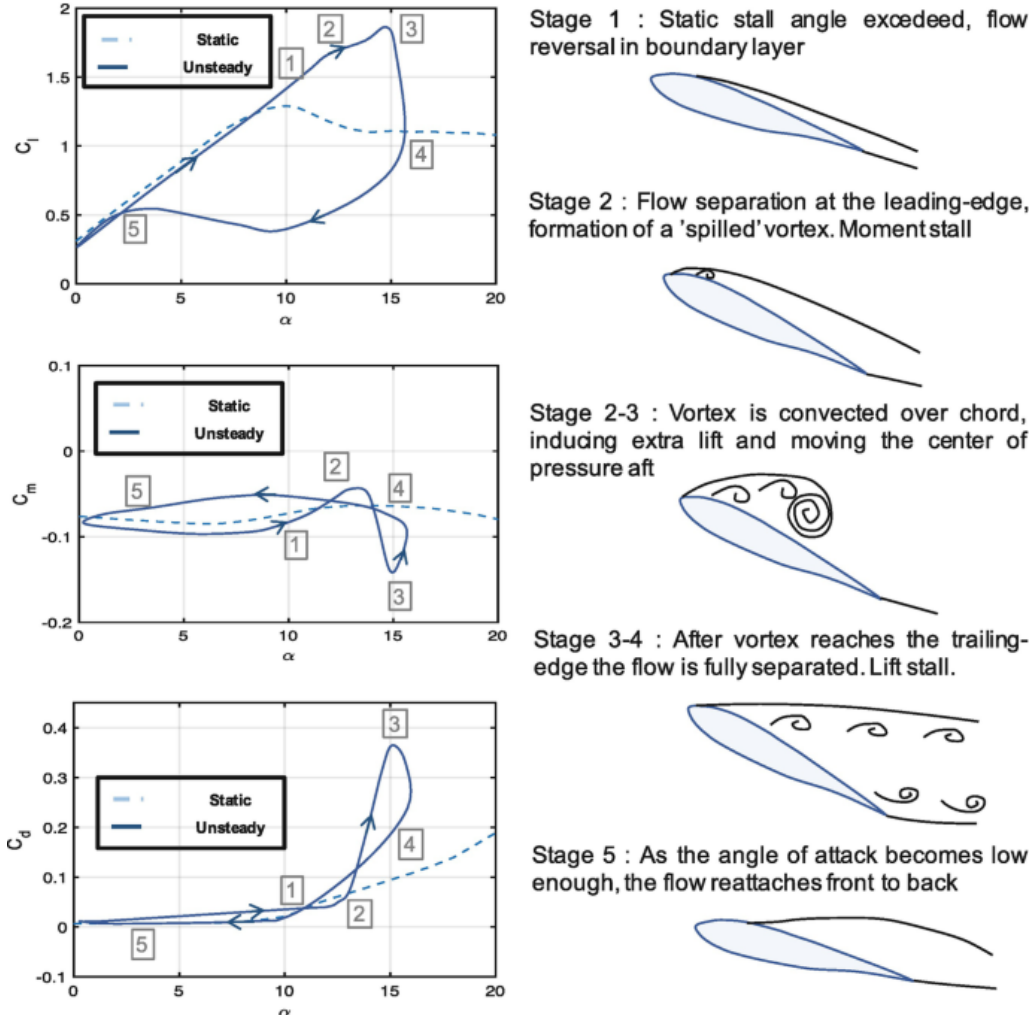
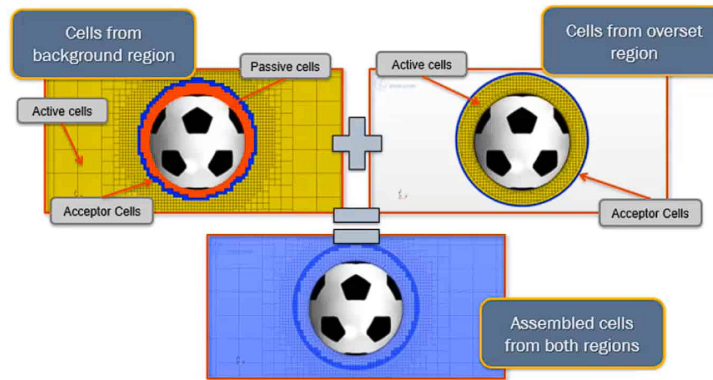


Figure 2.5: Dynamic stall stages taken from literature

## 2.6 Overset Mesh

Overset mesh is a method using (at least) two different computational grids, and allowing the grids to overlap and transfer flow field information between the grids. Usually, one mesh describes the whole computational domain (background mesh), and the other mesh describes the mesh for a smaller part of the domain that is moving with a moving object (overset mesh). The background mesh is usually quite coarse while the overset mesh is refined, since the moving object may need a customized refined mesh to predict the more complex flow field around it. An example overset mesh application where it is used to simulate motion of a football is shown in Fig.2.6. [11].



**Figure 2.6:** Overset mesh example from literature: Overset mesh setup for football moving in air

Overset grids are particularly useful for simulations involving moving components or dynamic interactions. By allowing independent motion of overlapping grids, overset mesh facilitates the simulation of complex fluid-structure interactions, such as rotating or translating components.

## 2.7 Boundary Conditions Used in Simulation

### 2.7.1 Stagnation Inlet

The stagnation inlet boundary is an inlet condition that is well-posed for compressible flows, although it is equally valid for incompressible flows. The stagnation conditions refer to the conditions in an imaginary plenum, far upstream, in which the flow is completely at rest. For incompressible flows, Bernoulli's equation is used to relate total pressure, static pressure, and velocity magnitude. Commonly used as the inlet to a simulation of internal flows for which the stagnation conditions are known.

### 2.7.2 Pressure Outlet

The pressure outlet boundary is an outflow condition that imposes the working pressure. This boundary pressure can be considered as the static pressure of the environment into which the fluid enters. The working pressure is always expressed relative to the reference pressure. It represents the difference between the absolute pressure and the reference pressure.

## 2.8 $k - \omega$ Turbulence Model

The  $k - \omega$  turbulence model is a two-equation model that solves transport equations for the turbulent kinetic energy  $k$  and the specific dissipation rate  $\omega$ —the dissipation rate per unit turbulent kinetic energy in order to determine the turbulent eddy viscosity. The standard  $k$  model is a low  $Re$  model, i.e., it can be used for flows

with a low Reynolds number where the boundary layer is relatively thick and the viscous sub-layer can be resolved. Other advantages include a superior performance for complex boundary layer flows under adverse pressure gradients and separations (e.g., external aerodynamics and turbo machinery).

## 2.9 Drosophila Melanogaster (Fruit Fly)

The fruit fly *Drosophila Melanogaster* is capable of impressive aerial maneuvers, hovering, fast movement, and balancing while moving through the air. This performance is due to a set of muscles, exoskeleton structures, and wings known as the flight motor[19]. Studies also found that the number of muscles involved in carrying out such complex motions is significantly low in fruit flies compared to other hovering insects[3]. The key to understanding how these flies control their flight lies in their complex wing hinge and flight motor. During the flapping motion, fruit flies move their wing at a high angle of attack which causes flow to separate and generate vortices. The difference in the pressure between upper and lower wing surfaces enhanced by the generation of vortices creates the lift force required to hover and fly. Fig.2.7 shows the photograph of a fruit fly[8].



**Figure 2.7:** *Drosophila Melanogaster* (Fruit Fly)

### 2.9.1 Fruit Fly Wing Kinematics

The fruit fly kinematics used in the study is taken from literature [18]. The spatial orientation of the wing defined by Euler angles as well as the translatory position of the wing root in space as a function of time constitutes the wing kinematics discussed in the work. Perl et al[18] in their work explain the procedure used to record the fruit fly kinematics using high-speed imaging. They observed the kinematics of hovering motion in detail and recorded the trajectories traced by the wing root and wing tip. Maya et al.[14] in their work did a similar approach recording the kinematics of the fruit fly wing in hovering motion. And utilized a three-dimensional hull reconstruction approach to identify the pose of the fly's body and wings with respect to time. The kinematic data is fitted using Fourier series approximations with 5-8 terms depending on the variable. Wing beat frequency and fluid domain properties are taken from work by Pons et al [19]. The fruit fly wing tip and root

trajectories plotted using the Fourier series approximations are shown in Fig.2.8. and Fig.2.9.

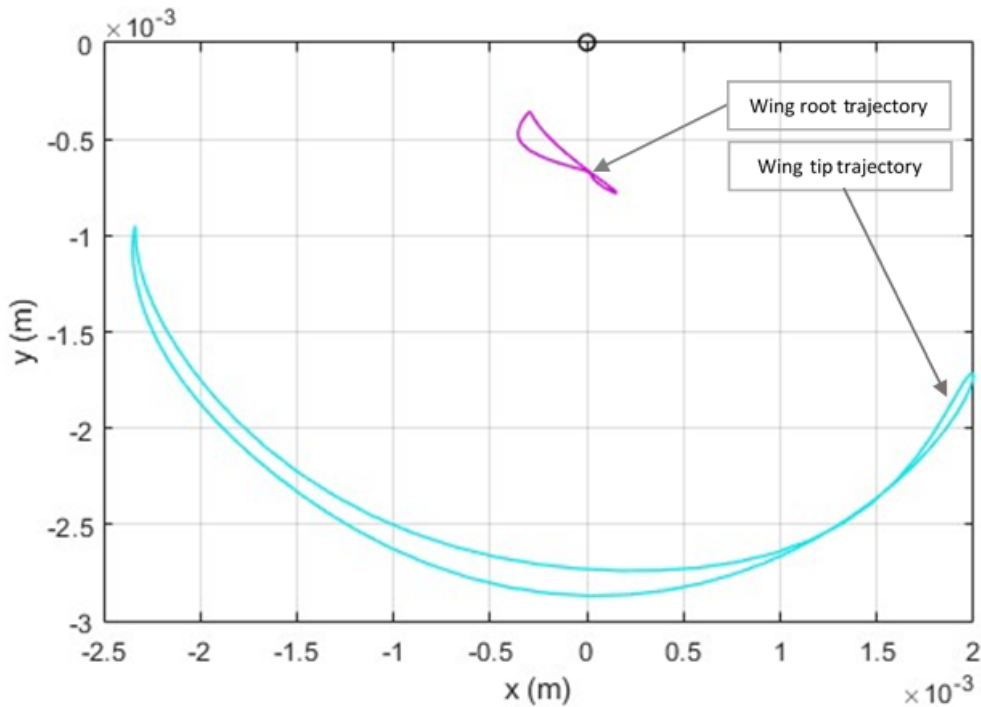


**Figure 2.8:** Drosophila Melanogaster Wing Trajectory (top view)

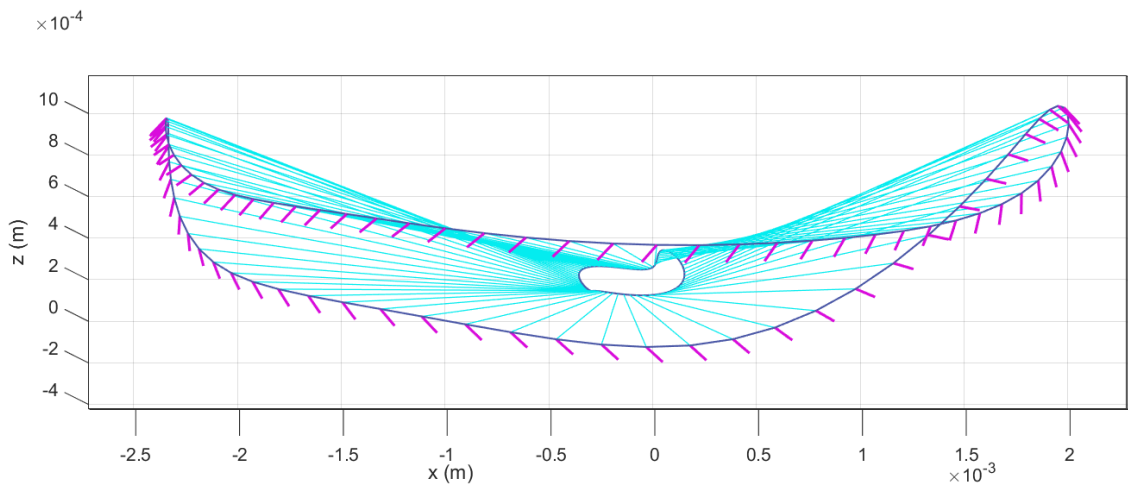


**Figure 2.9:** Drosophila Melanogaster Wing Trajectory (Wing tip view)

The coefficients of Fourier series approximations used for root trajectory and Euler angle variation for left and right wings are shown below.

## 2. Theory

---

```
%Fourier coefficients:  
rootCoeffsX = [0.0028929,0.010545,-0.00028184,-0.0008893,  
    0.0020166,-0.00069295,0,0,0,0,0,0,0,0,0,0];  
  
rootCoeffsY = [-0.0043044,-0.0072242,0.0013097,0.0024587,  
    -0.00040197,4.6619e-05,0,0,0,0,0,0,0,0,0];  
  
rootCoeffsZ = [0.0038606,0.0011476,-0.0010172,0.00095483,  
    -0.0012684,-0.00022335,0,0,0,0,0,0,0,0,0];  
  
phiL_coeff = [ 100.8025    73.0880     3.2347    -1.5820    -0.9568  
    4.2585    -0.7202    -1.2631    -0.7062     0.0769     0.4805 ];  
  
phiR_coeff = [ -100.8585   -73.8684    -5.1211     0.4147     1.8996  
   -3.0560     0.2620      0          0          0          0      ];  
  
psiL_coeff = [ 90.8299     9.3330    -61.6726     2.6201     7.0066  
  14.7058    -5.2175    -4.1670    -2.3880     2.0205     6.3990    -0.2757  
  -0.6554    -2.0145     0.0945     0.2967    -0.9058 ];  
  
psiR_coeff = [ 89.4874     3.0351    -64.5055     0.0464    -1.3748  
  14.3808    -8.7732    -0.0201    -5.2505     2.0074     5.6297     0.3232  
  3.0176    -3.2268     1.1359    -1.8282     0.0011 ];  
  
thetaL_coeff = [ 21.0851     2.1207     1.5256     9.4504     4.3725  
  -0.2600    -2.8082     0.4083     1.7483      0          0      ];  
  
thetaR_coeff = [ 18.5406     3.0000     2.9889     6.6285     4.2808  
  0.2547    -2.3093     0.0340     1.0105      0          0      ];
```

# 3

## Methodology

Computational Fluid Dynamics (CFD) serves as a tool for studying fluid dynamics problems with high fidelity. The basic CFD workflow involves pre-processing, solving, and post-processing. In this chapter, we have outlined the CFD workflow that we followed to simulate the unsteady aerodynamics of fruit fly wing beat motion in STAR-CCM+.

As mentioned in the introduction, we follow an approach to simulation where we consider the wing as rigid. In the pre-processing section preparation of geometry and computational domain, the dataset for simulating kinematics, and the generation of computational grid required for simulation are discussed. Further physics for the simulation is set up and solved with the aid of cluster computing platforms. In the final step of post-processing, results from the simulation are consolidated for analysis.



---

**Figure 3.1:** Fruit fly wing geometry

### 3.1 Pre-Processing

#### 3.1.1 Geometry Preparation

The fruit fly wing geometry used in the simulation is taken from literature[18]. According to Perl et al, The wing's shape and size were determined by calculating the polygon defined by ten designated wing landmarks. These landmarks facilitated the acquisition of wing coordinates, forming the basis for the subsequent computation of wing shape and surface area. The primary components of variation in shape

were defined from the landmark data. This involved employing Procrustes superimposition on the landmark data, which encompassed reflection, scaling (utilizing centroid size), and rotation. These transformations were applied to align the wings, minimizing deviations from the overall mean shape. Consequently, this systematic procedure enabled the characterization of shape variations within the wings. The CAD geometry imported to the STAR-CCM+ software is shown in Fig.3.1. The wing geometry is scaled such that the wing span measures 2.5mm. Also to ensure that the initial position of the root matches with the trajectory, the origin of the CAD geometry is defined at the root itself while importing to STAR-CCM+.

#### 3.1.2 Wing Kinematics Dataset for Simulation

To define the wing beat motion in STAR-CCM+, a set of Euler angles and spatial coordinates of the wing root is derived from the Fourier series approximations. The wing beat frequency of 218 Hz was considered and the entire cycle time was discretized into 1000 instances. With the help of MATLAB, time series data of Euler angles and root position is generated and stored as tabulated files. The coordinates of the root in the dataset are modified such that the initial set of root coordinates corresponds to the origin of the wing which is positioned at its root. This is done by subtracting the root coordinates obtained while importing the wing to STAR-CCM+ from all the sets of root coordinates in the dataset. By doing this modification, we can ensure that the root will be positioned at the desired position from the set of root trajectory coordinates we have in the dataset. The dataset used for specifying motion is given in the Appendix 1 section.

#### 3.1.3 Computational Domain and Grid Generation

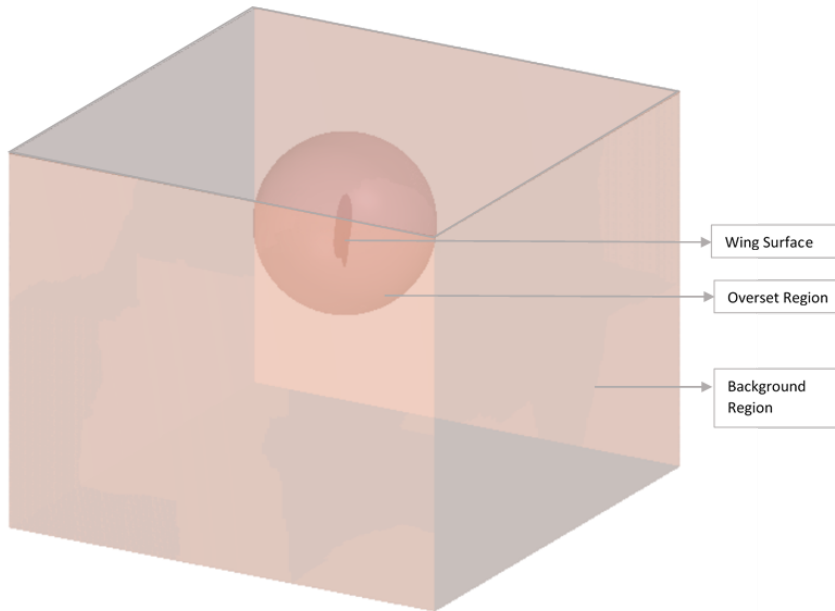


**Figure 3.2:** Computational domain used in simulation

The computational domain consists of two regions namely background region and overset region and is shown in Fig.3.2. The overset region is generated by subtractive boolean operation of the wing geometry from an initial sphere part. The span of the fruit fly wing geometry considered is 2.5 mm. Accordingly, the background region is sized to be 8 times larger in dimensions to avoid any boundary influence. The overset is centered approximately at the geometric center of the wing. Workflow followed to create the computational domain is shown in Fig.3.3.

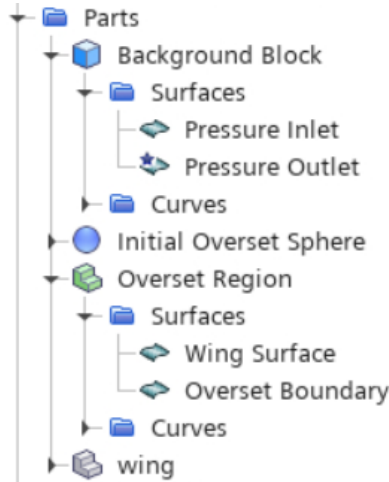


**Figure 3.3:** Steps to create computational domain

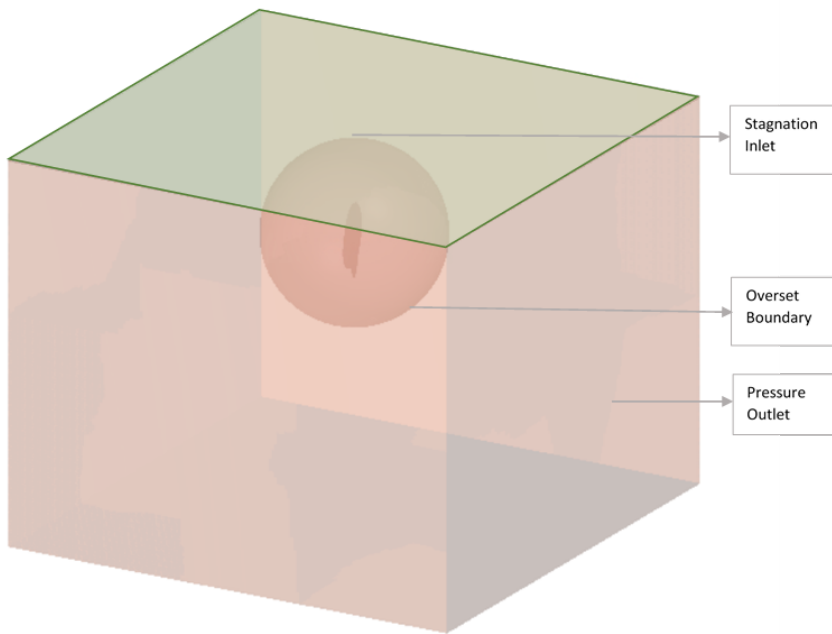


**Figure 3.4:** Boundary conditions used at various region boundaries

From the computational domain, regions and corresponding boundaries are created. Stagnation inlet boundary condition is used to define the top boundary of the background region. Since we are simulating the hovering phase of flight, stagnation

### 3. Methodology

---

inlet condition is used to specify zero velocity at the top boundary and atmospheric pressure. The other boundaries of the background region are defined using pressure outlet conditions. The overset region is defined as the overset mesh type and the boundary between the overset region and the background region is created as an overset boundary. The overset boundary is later used to define the overset mesh interface. The different boundary conditions used at various boundaries of the two regions are shown in Fig.3.4.

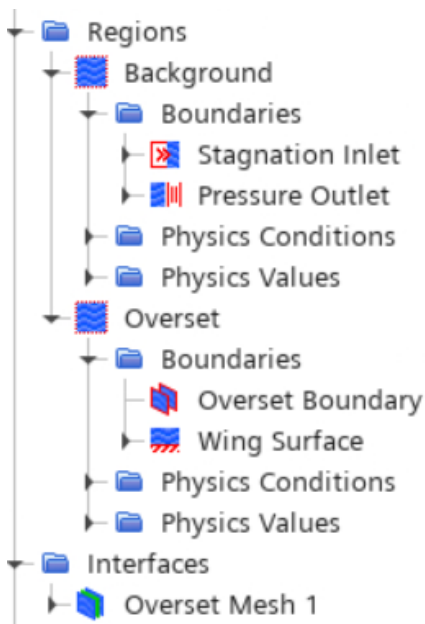


**Figure 3.5:** Steps to setting up boundary conditions

A grid independence study was not done for this work. The mesh settings are taken from experience. And the computational resources permitted us to generate and use a uniform fine mesh. The base size for the background regions was set as 0.1 mm. The target size for the overset boundary was also kept at 0.1 mm in size. The minimum surface size for the overset region used is 0.005 mm and a very slow volumetric growth rate was chosen inside the overset region.

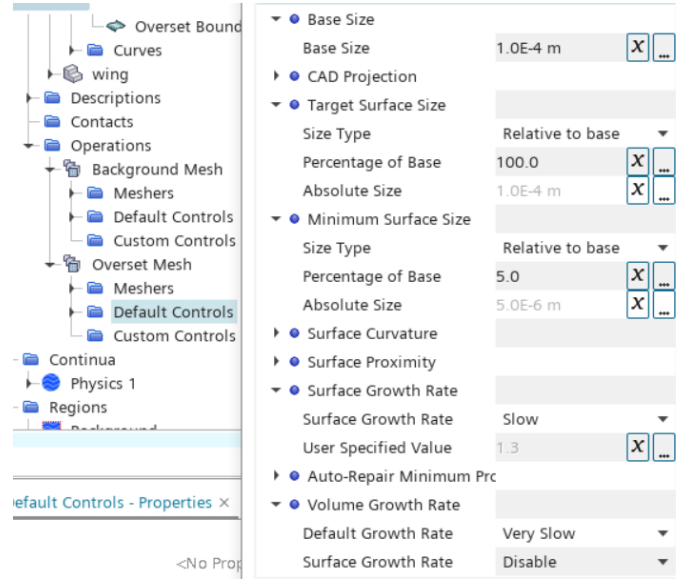


**Figure 3.6:** Mesh control for overset mesh

The overset mesh has to replace the mesh region of the background at each time step since the overset is in motion. The entire mesh cannot be updated each time as it is computationally expensive and time-consuming. To overcome this alternate hole cutting region is defined to the overset mesh. This makes the overlapped mesh region from the background be removed from computation during the motion. This necessitates the mesh size to be uniform and of similar order at the interface between the overset and background. Adaptive Mesh Refinement (AMR) setting is used to smoothen the interface between overset and background during each time step. The default controls used to set up the overset mesh are shown in Fig.3.6. The generated computational grid is shown in Fig.3.7. A section view showing the overset region is shown in Fig.3.8.

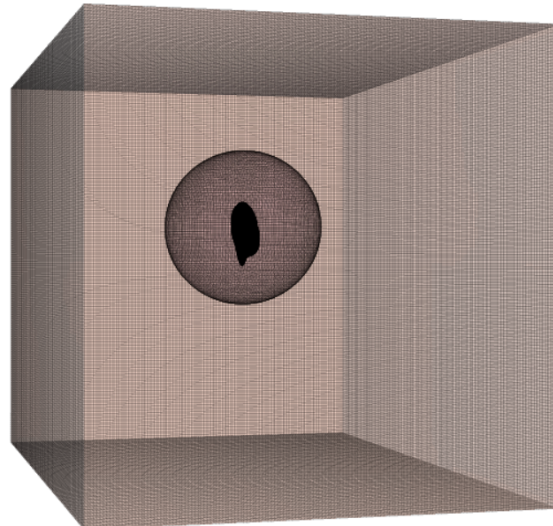


**Figure 3.7:** Computational grid

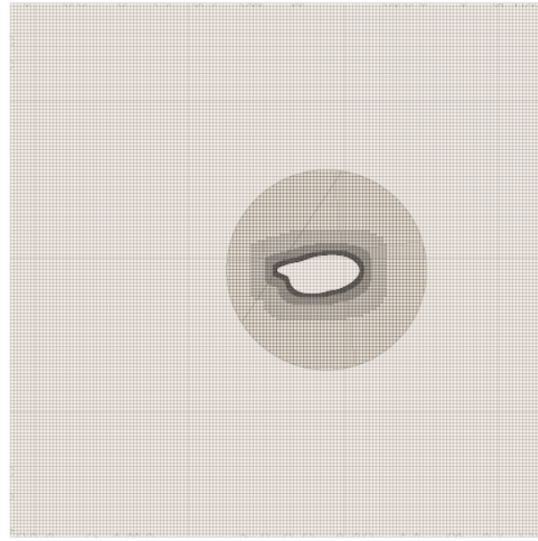


**Figure 3.8:** Computational grid section view

### 3.1.4 Setting Up Wing Beat Motion in STAR-CCM+

In order to define the motion of the wing relevant coordinate systems are defined initially. The root trajectory of the wing is defined with respect to the laboratory coordinate system. In order to establish translation of the wing root along the defined trajectory, a coordinate system named *Trajectory* is used. Further to specify the Euler angles rotating local coordinate systems are defined to the translating *Trajectory* coordinate system. The image showing the Laboratory coordinate system and translating *Trajectory* coordinate system positioned at the wing root along with the highlighted root trajectory is shown in Fig 3.9.

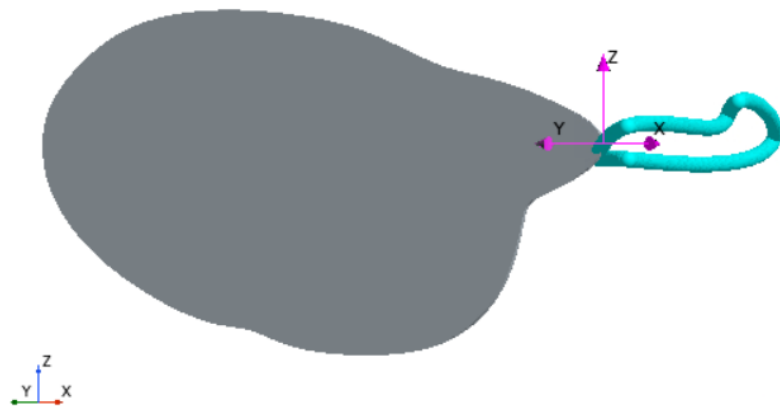


**Figure 3.9:** Laboratory and translating root-based Trajectory coordinate systems

The local coordinate systems to *Trajectory* are named *Yaw*, *Pitch* and *Roll*. The stroke angle is defined with respect to the *Yaw* coordinate system. The pitch angle

is defined with respect to the *Pitch* coordinate system and the elevation angle with respect to the *Roll* coordinate system. The tree showing the different coordinate systems used is shown in Fig 3.10. The superimposed rotational coordinate systems are shown in Fig 3.11.

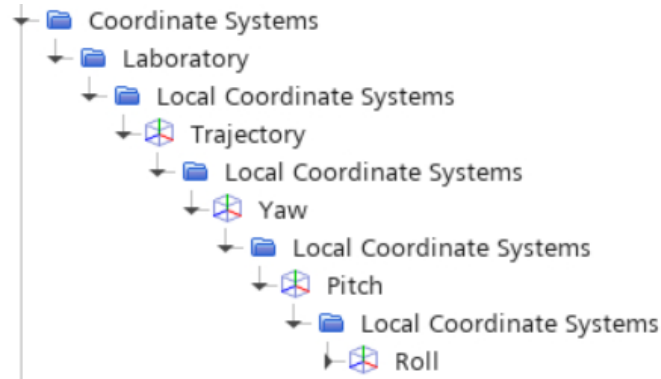


**Figure 3.10:** Coordinate systems used to define motion

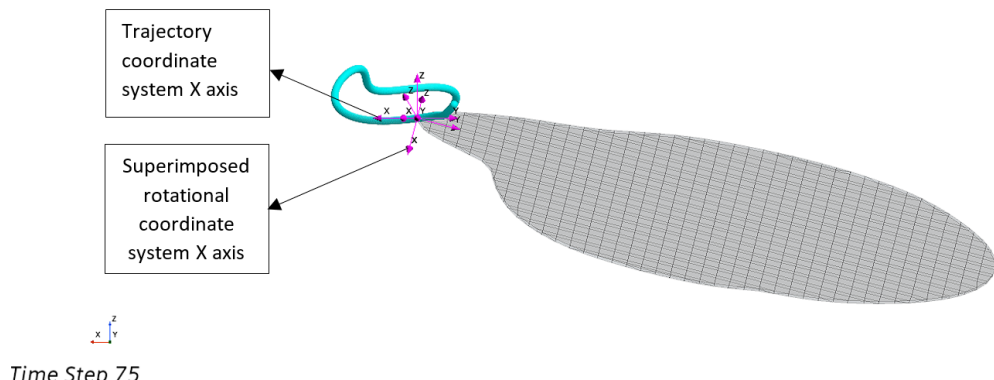


**Figure 3.11:** Superimposed coordinate systems used to rotational motions

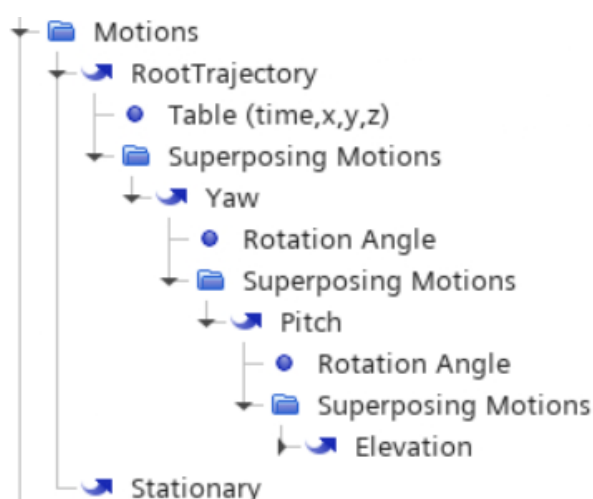


**Figure 3.12:** Define translation and superimposing rotations

### 3. Methodology

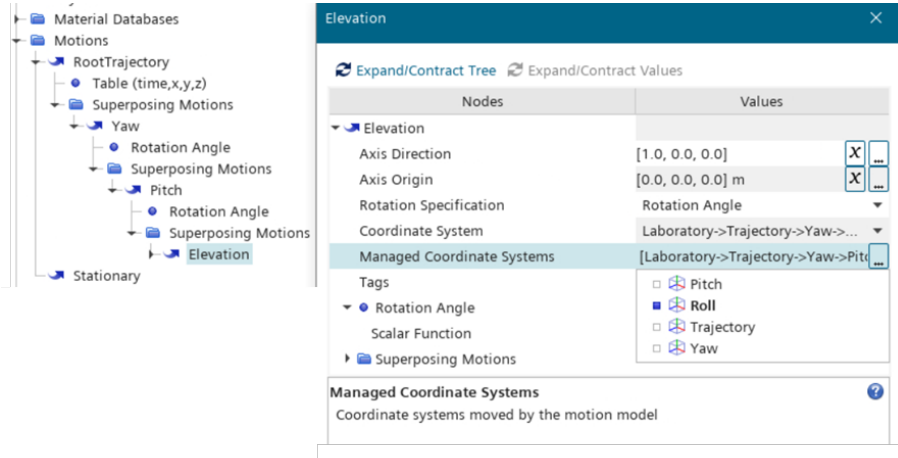


**Figure 3.14:** Superimposed motion parameters

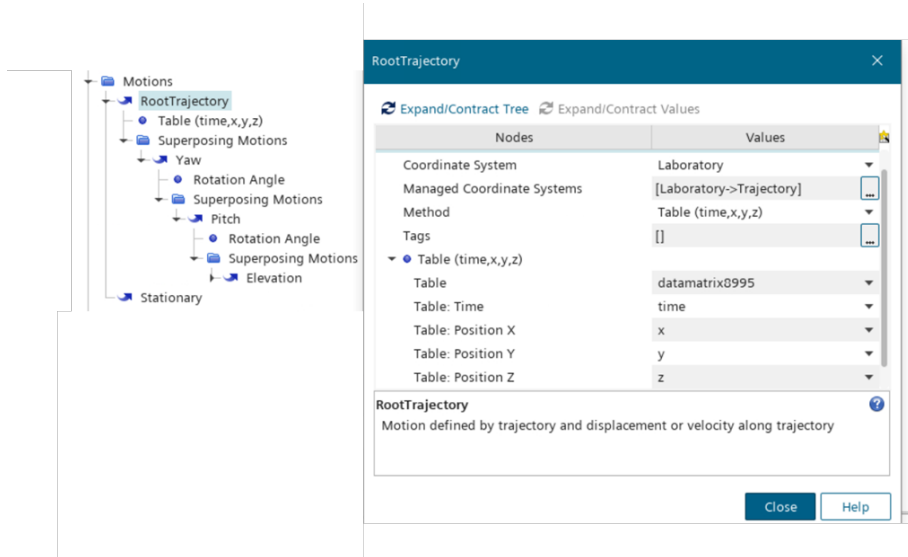


**Figure 3.13:** Root translation parameters

Using the different coordinate systems translation and rotations of the wing are defined. The combined translation and rotation motion is then assigned to the overset region. The positional and Euler angle data from the dataset is plugged into corresponding coordinate systems. This step is achieved using the *Motions* node in STAR-CCM+. The procedure for specifying the motion to the overset region is shown step by step in figures Fig 3.12, Fig 3.13, Fig 3.14.

While defining the translation to the trajectory as in steps from Fig.3.13, The motion is managed by a *Trajectory* coordinate system whose translation position along the trajectory is defined with respect to the global *Laboratory* coordinate system. The root coordinates are plugged in as a time position table. In a similar fashion, the superimposed rotations are also defined. Fig.3.14 shows the parameters set for this.

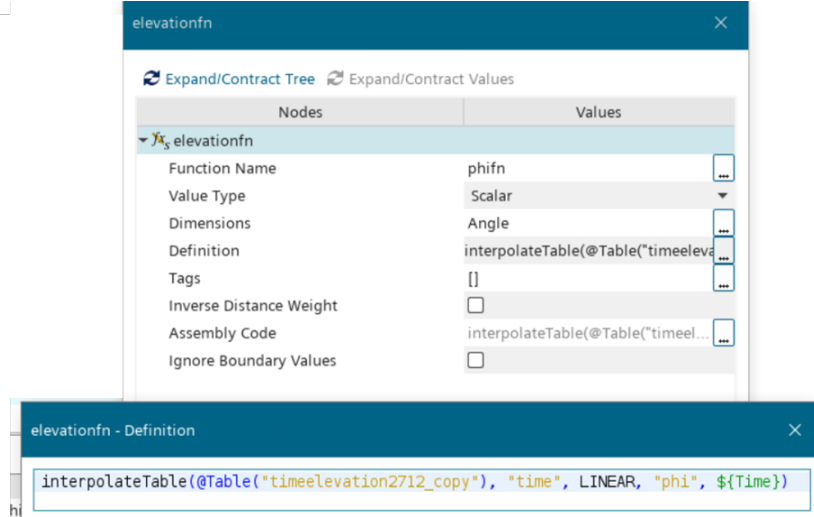


**Figure 3.15:** Rotation angle scalar function

The axis of rotation corresponding to the local coordinate system is set. Also, the motion is managed by the respective local coordinate system. In the case of the elevation motion, The reference coordinate system is the *Pitch* coordinate system, and the managed coordinate system is the *Roll* coordinate system. The rotation angle is given as a scalar function of time. The scalar function is defined in the *Fieldfunctions* node using the time series table for elevation angle. The syntax used to define the interpolation scalar function named *elevationfn* is given in Fig 3.15. The pitch and yaw motions are defined similarly. Once the motions are defined they are assigned to the overset region in its *motion\_specification*. This is shown in Fig 3.16.

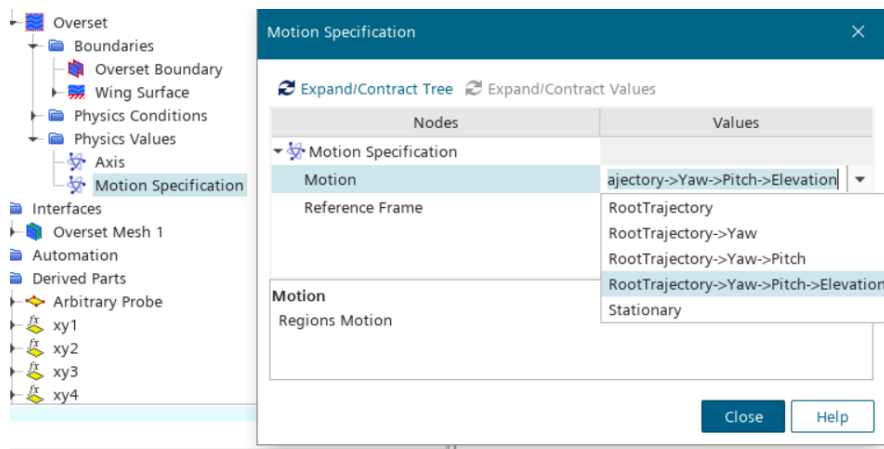


**Figure 3.16:** Motion specification to overset region

## 3.2 Physics and Solver Setup

Since the observed Reynolds number with the flow field surrounding the fruit fly wing is low and magnitudes near 100, An incompressible flow field is assumed. The

### 3. Methodology

---

k-omega turbulence model is enabled for better resolution of flow separation effects. The implicit unsteady solver with a time step equal to  $4.58\mu s$  is also used. This time step corresponds to 1/1000 of the cycle time for fruit fly wing beat. Further as mentioned before, Adaptive mesh refinement is used to carry out overset mesh interface refinement. The physics setup for the simulation is shown in Fig 3.17. The simulation was done for 8 wing beat cycles using a cluster computing platform.

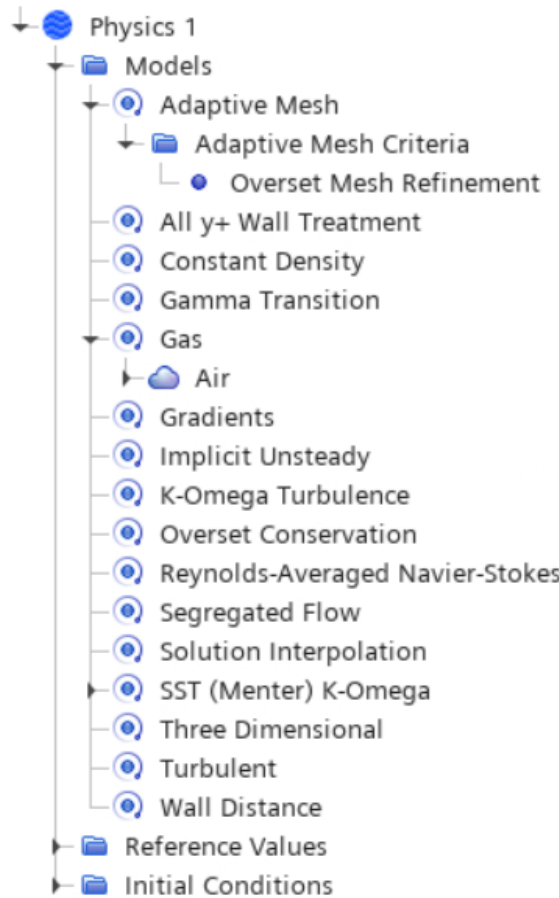


**Figure 3.17:** Physics setup

## 3.3 Post-Processing

To study the passiveness of pitch and stroke motions, we were particularly interested in recording the variation of the wing's pitching moment with respect to pitch angle as well as the variation of stroke moment with respect to stroke angle for each time-step. For this monitors of pitching moment and stroke moment are added to post-process. Also, the lift and drag characteristics of the wing over the cycle are also plotted. Velocity contours of the flow field are also captured as scenes. From the monitored data finally, hysteresis plots for pitch and stroke motions were generated for analysis.

The workflow followed in the work for carrying out the CFD simulation is based

on Simcenter STAR-CCM+ documentation:

*Trajectory\_Motion – Paint\_Dipping\_of\_a\_Chassis\_on\_a\_Fixed\_Skid*

### 3. Methodology

# 4

## Results & Summary

### 4.1 Wing Beat Cycle Motion Analysis

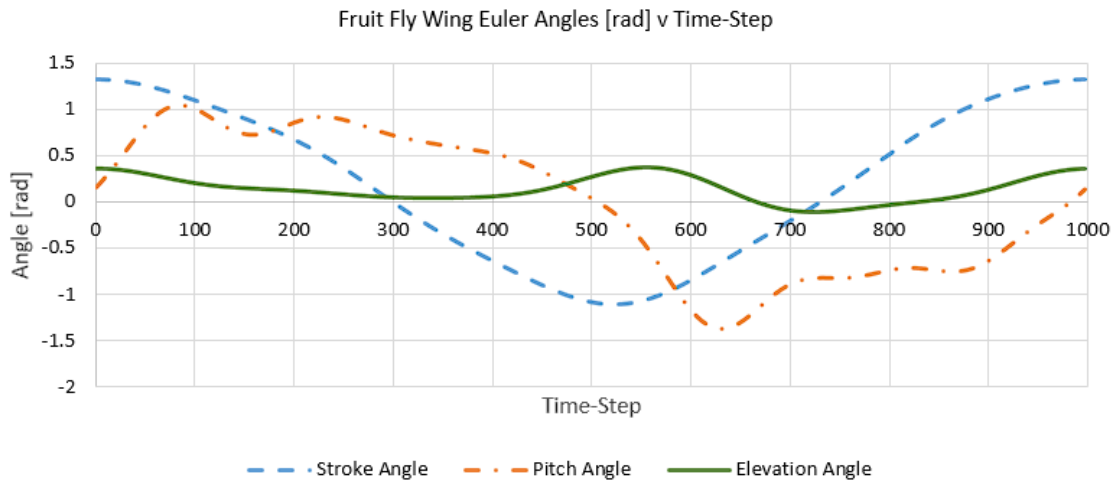


**Figure 4.1:** Variation of fruit fly wing Euler angles across wing beat cycle

Before the discussion of results, initially, the discretization of the wing beat cycle and analysis of the kinematic wing beat motion are presented. By tracking the orientation of the wing according to the kinematics, different maneuvers carried out by the wing are tried to understand. The variation of the fruit fly wing Euler angles derived from the kinematics [14, 18], measured with respect to the root coordinate system is plotted against time-step over a cycle in Fig 4.1.1.

The entire cycle of wing beat motion is discretized into 1000 time steps starting at T0 and ending at T1000. The frequency of wing beat considered for the study is 218 Hz [14, 18]. The time-step considered is 1/1000 of the cycle time.

As we break down the wing beat motion into different time steps, the cycle is assumed to start from the extremum of the backward stroke at T0, and the forward stroke happens till the wing reaches the extremum of the forward stroke near T500. While near the extremum of the forward stroke, the pitch angle continuously changes from obtuse to acute. A similar change of pitch angle, this time acute to

## 4. Results & Summary

---

obtuse happens at the end of the backward stroke. The pitch angle changes at the extremum orienting the fruit fly wing at a positive angle of attack during both forward and backward strokes.

The elevation angle of the wing has its local maxima while reaching the extremities of strokes. Also, the peculiar variation of the three angles during the extremities collectively depicts the flipping maneuver carried out by the fruit fly wing.

### 4.2 Aerodynamic Characteristics of Fruit Fly Wing Beat Motion

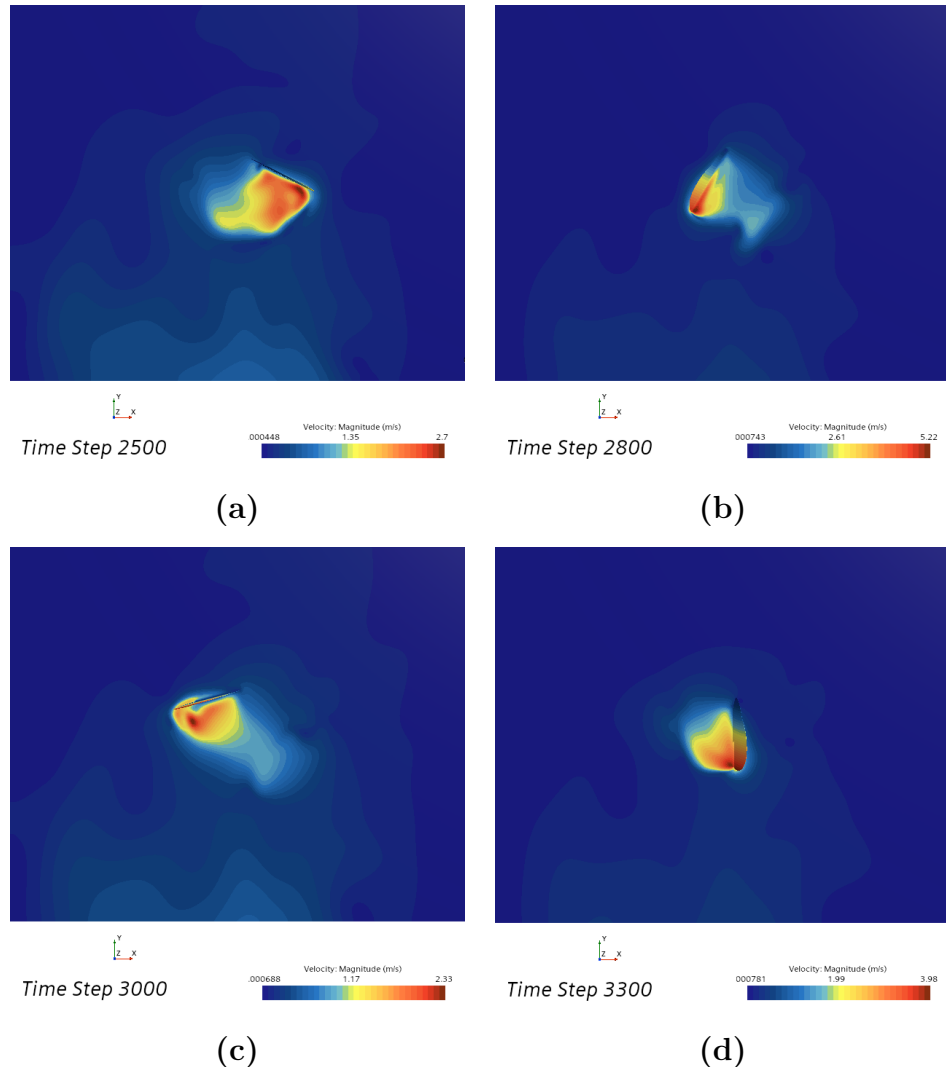


**Figure 4.2:** (a) Extremum of backward stroke (b) Intermediate position of forward stroke (c) Extremum of forward stroke (d) Intermediate position of backward stroke

The aerodynamic characteristics of the fruit fly wing motion obtained from CFD simulation are presented and discussed in this section. Eight wing beat cycles were simulated using CFD, and the results recorded for cycles 4 to 7 are used for interpretation. Since we are interested in the characteristics of the stabilized hovering motion of the fruit fly, the initial cycles are skipped. While observing the velocity field from CFD over different cycles, the flow field seemed to stabilize after 2 cycles.

Velocity contour of the flow field, variation of lift and drag over the wing beat cycle, pitching moment, and stroke moments are recorded for the specified cycles. The velocity contour taken on the z-plane at the mid-chord position of the wing recorded for different instances along the wing beat cycle is shown in Fig 4.2.1.

#### 4.2.1 Lift & Drag Characteristics

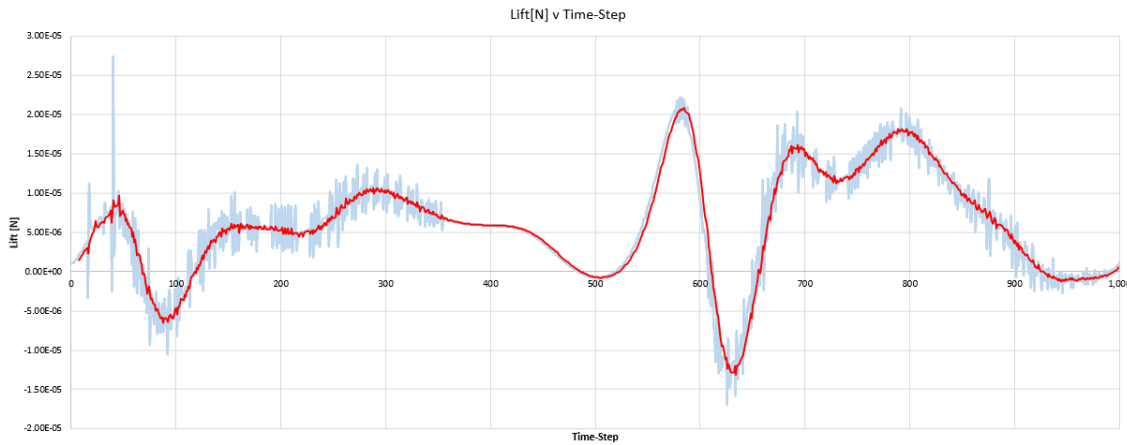


**Figure 4.3:** Lift profile over wing beat cycle

The variation of lift generated by the wing over the wing beat cycle is plotted in Fig 4.2.2. The calculation of lift is made with respect to the stationary laboratory coordinate system. A moving average is used to smoothen the profile and an average is considered. The maximum of the lift profile is observed to be near T600. This region corresponds to the extremum of the forward stroke and is characterized by the pitch angle reversal. The fruit fly wing flips to orient itself at a positive angle of attack in preparation for the backward stroke. The eddies created by this complex motion as well as the low pressure created by the tail flow might have resulted in this peak lift. When we take the average lift over the entire cycle, a positive lift with a magnitude equal to  $5.76 \mu N$  per wing is observed. The mass of fruit-fly is considered to be equal to  $1.2 mg$  [16] and the lift produced corresponds to a lift-to-weight ratio approximately equal to 1. Considering the hovering motion of the fruit fly, the calculated lift-to-weight ratio being equal to one suggests reasonable adherence between simulated aerodynamic characteristics and reality.

## 4. Results & Summary

---

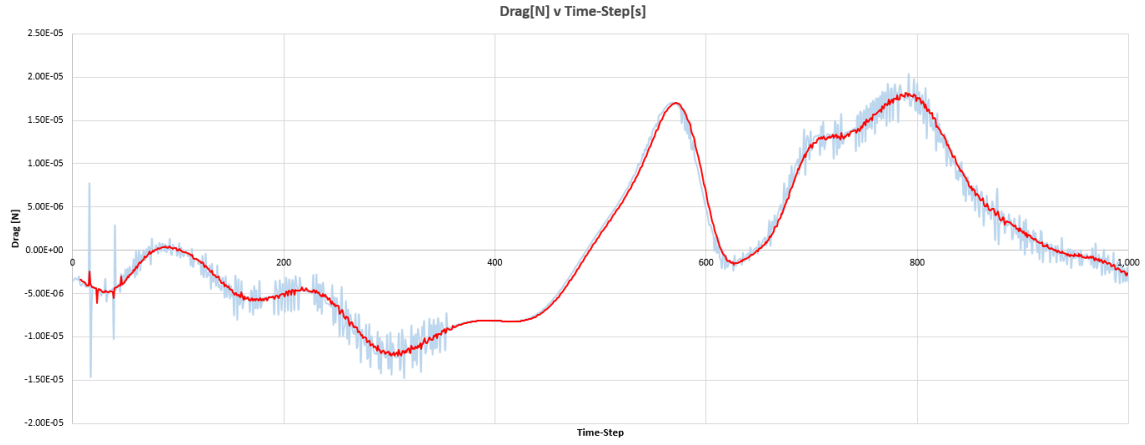


**Figure 4.4:** Drag profile over wing beat cycle

The drag profile plotted for the wing beat cycle is shown in Fig 4.4. Similar to lift calculation the drag over the wing is measured with reference to the laboratory coordinate system. During the pitch reversal, the wing orient itself vertically at some point. This corresponds to the maximum drag point. The relative velocity of the backward stroke is higher compared to the forward stroke. This can result in a relatively high lift-induced drag. The similarity in lift and drag profile indicates this. The average drag measured over an entire cycle is  $0.8 \mu N$ . The observed drag over the entire cycle is minimal.

### 4.2.2 Pitching Moment & Stroke Moment Characteristics

In this section, the pitching moment and stroke moment characteristics of the wing are studied. By evaluating the different moments exerted by the aerodynamic forces over the wing, the requirement for active involvement of fruit fly wing muscles is investigated.

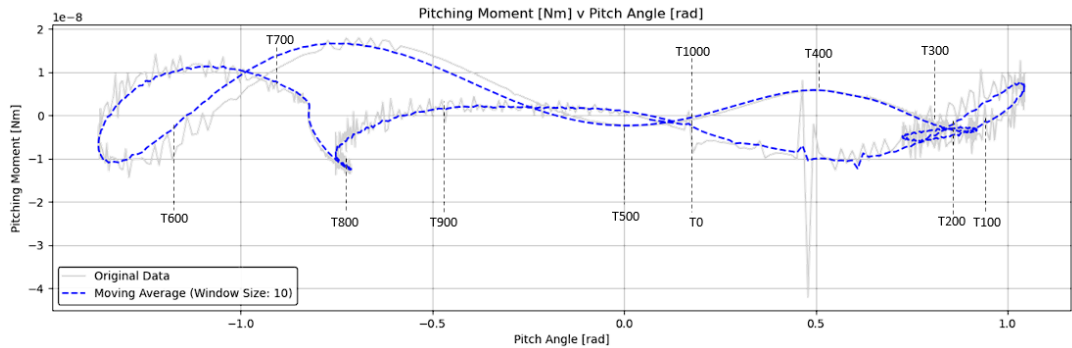


**Figure 4.5:** Pitching moment with respect to pitch angle variation over cycle

The pitching moment evaluated with respect to the wing root coordinate system is plotted against the pitch angle in Fig 4.5.

The absolute area inscribed by the pitching moment hysteresis loop is depicted in Fig 4.6. The magnitude of the absolute area inscribed is  $-2.56 \text{ nJ}$ . The observed overall cycle hysteresis is negative which indicates insignificant energy expenditure over the complete cycle. Even though hysteresis over the complete cycle is near zero, we can observe the curve to self-intersect at different instances along the forward and backward strokes.

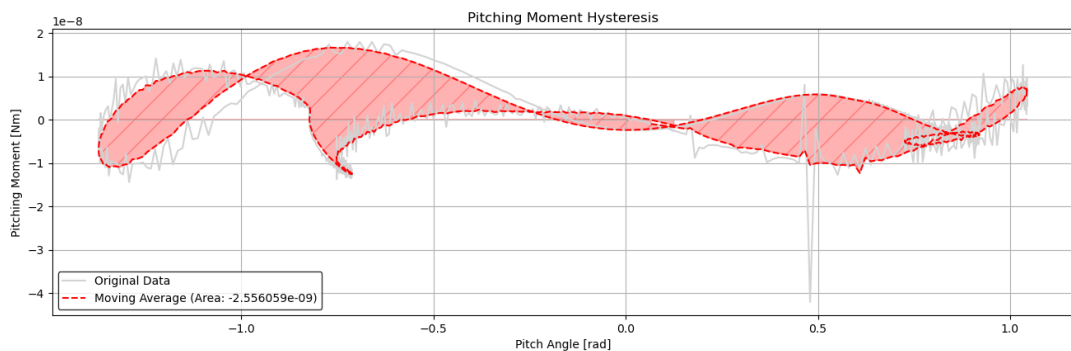


**Figure 4.6:** Pitching moment hysteresis over a cycle

The dissipators like muscle tissue in insects are characterised by a continuous hysteresis loop [15]. The self-intersecting curves indicate the involvement of muscles in the pitch motion. Also, the reversal of the loop observed near T600 can be a scenario of dynamic stall and vortex shedding since the wing is in near vertical orientation and beyond normal stall angle [4]. The dynamic stall seems to continue till T800 where the sharp region is observed. Beyond this point, a relatively stable variation of pitching moment is observed. This indicates the flow getting re-attached to the wing. As we observe the instances after the extremum of a backward stroke at T100, a rather complex profile is observed. Between T100 and T300 the curve intersects itself twice. The variation of pitch angle in this region is rapid and this can also be a case of flow separation and dynamic stall. The regions of significant hysteresis are in common characterised by the pitch angle reversal. As also seen in the pitch angle variation in Fig 4.1, the pitch angle seems to be almost steady in between the stroke extremes and with a peculiar waviness.

When comparing the pitching moment profile with lift data, we can observe that the local maxima of lift seem to match the regions of pitching moment reversal. This is indicative that the vortex shedding made by the rapid variation in pitch angle is aiding the lift generation by the wing.

## 4. Results & Summary

---

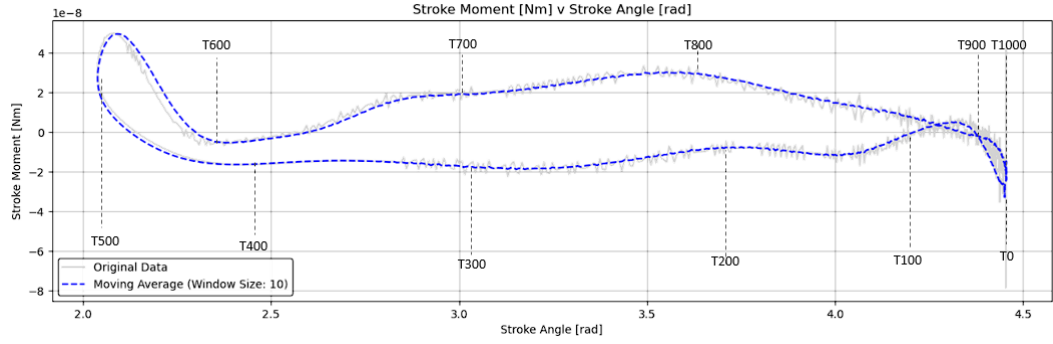


**Figure 4.7:** Stroke moment with respect to stroke angle variation over cycle

The stroke moment evaluated with respect to the wing root coordinate system is plotted against the stroke angle in Fig 4.7. The stroke moment hysteresis over the cycle is shown in Fig 4.8. The observed variation is similar to those found in literature [19].

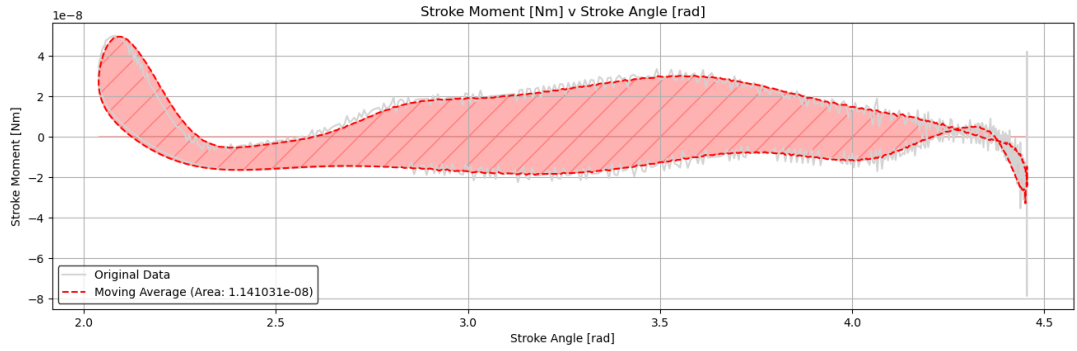


**Figure 4.8:** Stroke moment hysteresis over a cycle

While analyzing the stroke moment variation, we can notice significant variations near the extremes of strokes. At T0 where the backward stroke ends, the curve is intersecting and the moment value is undergoing a sudden drop. This indicates dynamic stall and vortex shedding. Between T500 and T600 also there exists a noticeable increase in stroke moment. Unlike the variation at T0, the variation at the end of the forward stroke is less rapid and relatively smooth.

The absolute area of the hysteresis loop is positive and this indicates that work is done by the wing during the stroke motion. The magnitude of the hysteresis loop area is 11.4 nJ.

### 4.3 Summary

The complex unsteady maneuver of the wing at the extremities of forward and backward strokes creates significant variations in pitching moment and stroke moment characteristics.

The stroke motion hysteresis underlines the active nature of stroke motion. Self-intersecting behavior of the pitching moment curve indicates active involvement of insect muscles during pitch reversal. Also, the nature of the variations in pitching moment and stroke moment indicate that the wing is subjected to dynamic stall during pitch reversal. Even though there is a noticeable variation in lift and drag at these positions, sufficient average lift is maintained by the wing. We observed an increase in elevation angle accompanying the pitch reversal. While this maneuver may aid the pitch reversal process, it might also compensate for the decrease in lift due to stall. Apart from the extremities of the cycle, pitch motion seems to be passive with minimal hysteresis involved. To summarize, even though hysteresis for the pitch motion adds up to a negative value, the pitch reversal process might be partially active either by contribution from a muscle or coupling from an active elevation motion.

The approach presented in the study considered the fruit fly wing as a rigid body. A fully coupled CFD simulation involving non-linear flexible wing effects can be a future scope of this project.

#### 4. Results & Summary

# Bibliography

- [1] Dickinson MH Balint CN. The correlation between wing kinematics and steering muscle activity in the blowfly *calliphora vicina*. *J Exp Biol.* 2001 Dec;204(Pt 24):4213-26, 2001.
- [2] Tsevi Beatus and Itai Cohen. Wing-pitch modulation in maneuvering fruit flies is explained by an interplay between aerodynamics and a torsional spring. *Phys. Rev. E*, 92:022712, Aug 2015.
- [3] Lorinda Dajose. Small but mighty: Fruit fly muscles. 2017.
- [4] Michael H. Dickinson, Fritz-Olaf Lehmann, and Sanjay P. Sane. Wing rotation and the aerodynamic basis of insect flight. *Science*, 284(5422):1954–1960, 1999.
- [5] Charles Porter Ellington and Michael James Lighthill. The aerodynamics of hovering insect flight. iv. aerodynamic mechanisms. *Philosophical Transactions of the Royal Society of London. B, Biological Sciences*, 305(1122):79–113, 1984.
- [6] Kolomenskiy D. Petrov P.N. et al. Farisenkov, S.E. Novel flight style and light wings boost flight performance of tiny beetles. *Nature* 602, 96–100, 2022.
- [7] Nicole George, Simon Sponberg, and T Daniel. Temperature gradients drive mechanical energy gradients in the flight muscle of *manduca sexta*. *The Journal of experimental biology*, 215:471–9, 02 2012.
- [8] Nicolas Gompel. Freak flies and miscellaneous. Technical report.
- [9] Johanna S. U. Hedlund, Hua Lv, Philipp Lehmann, Gao Hu, R. Charles Anderson, and Jason W. Chapman. Unraveling the world’s longest non-stop migration: The indian ocean crossing of the globe skimmer dragonfly. *Frontiers in Ecology and Evolution*, 9, 2021.
- [10] Sabrina Henne, Agastya Parikh, Julien Deparday, and Karen Mulleners. Dynamic stall vortex shedding and associated load fluctuations. In *19th International Symposium of the Applications of Laser and Imaging Techniques to Fluid Mechanics*, 2018.
- [11] Christoffer Johansson. Overset mesh in simcenter star-ccm+. 2021.
- [12] Muhammad Arsalan Khan. *Dynamic Stall Modelling for Wind Turbines*. PhD thesis, 08 2018.
- [13] Teaching material for student pilots of the Italian Air Force Academy. Aerodynamic pitching moment. Technical report.
- [14] Roni Maya, Noam Lerner, Omri Ben-Dov, Arion Pons, and Tsevi Beatus. A hull reconstruction-reprojection method for pose estimation of free-flying fruit flies. *Journal of Experimental Biology*, 226(21):jeb245853, 11 2023.
- [15] Khoi D. Nguyen and Madhusudhan Venkadesan. Rheological basis of skeletal muscle work loops, 2020.

## Bibliography

---

- [16] Lefkovitch.L. et al. Pecsenye.K., Bokor.K. Enzymatic responses of drosophila melanogaster to long- and short-term exposures to ethanol. enzymatic responses of drosophila melanogaster to long- and short-term exposures to ethanol. *Mol Genet* 255,258–268, 1997.
- [17] Murat Peksen. Chapter 5 - multiphysics modelling of interactions in systems. In Murat Peksen, editor, *Multiphysics Modelling*, pages 139–159. Academic Press, 2018.
- [18] Illy Perl, Roni Maya, Oron Sabag, and Tsevi Beatus. Lateral instability in fruit flies is determined by wing–wing interaction and wing elevation kinematics. *Physics of Fluids*, 35(4):041904, 04 2023.
- [19] Arion Pons, Illy Perl, Omri Ben-Dov, Roni Maya, and Tsevi Beatus. Solving the thoracic inverse problem in the fruit fly. *Bioinspiration Biomimetics*, 18(4):046002, may 2023.
- [20] J.W.S. Pringle. Comparative physiology of the flight motor. volume 5 of *Advances in Insect Physiology*, pages 163–227. Academic Press, 1968.
- [21] Ricardo Santos Pereira. *Dynamic Stall*, pages 331–351. Springer International Publishing, Cham, 2022.
- [22] Simon Walker, Adrian Thomas, and Graham Taylor. Operation of the alula as an indicator of gear change in hoverflies. *Journal of the Royal Society, Interface / the Royal Society*, 9:1194–207, 11 2011.

# A

## Appendix 1

In this investigation, we utilized the dataset for the study of unsteady aerodynamics of fruit-fly wing motion to assess the passiveness of different degrees of freedom. The dataset can be found in the following link:

1. Dataset for investigation of unsteady aerodynamics of fruit-fly wing motion to determine passiveness of different degrees of freedom